ACS OMEGA

http://pubs.acs.org/journal/acsodf

Article

Chelation-Based Route to Aluminum-Free Layered Transition Metal Carbides (MXenes)

Luis R. De Jesús Báez,* Alyssa S. Rosas, Pratibha Mahale, and Thomas E. Mallouk*

Cite This: *ACS Omega* 2023, 8, 41969−41976

Read Online

ABSTRACT: MXenes are of much interest because of their electrochemical, electronic, and surface chemical properties that arise from their structure and stoichiometry. The integrity and the nature of the terminal groups on the basal planes of MXene sheets depend strongly on the method used to etch the parent MAX (M = transition metal, A = Al, X = C, N, B) compound. Aluminum removal typically involves a high concentration of aqueous HF, HCl/LiF mixtures, or fluoride solutions of strong acids. HF etching is problematic because it leaves insoluble AlF_3 in the product, degrades the crystallinity of the nanosheets, and results in the termination of the basal planes with F, O, or OH groups. Here, we demonstrate the use of HF at a low concentration in tandem with a chelating agent, *N*,*N*′-dihydroxyoctanediamide (suberohydroxamic acid), to selectively etch the archetypical MAX compound Ti_3AlC_2 at room temperature. X-ray absorption spectroscopy (XAS) of the etched materials shows that the carbide nature of bonding in the parent MAX structure is retained in the MXene layers. The stability of the MXene in aqueous suspensions is also significantly improved relative to MXene products made by etching in concentrated HF solutions.

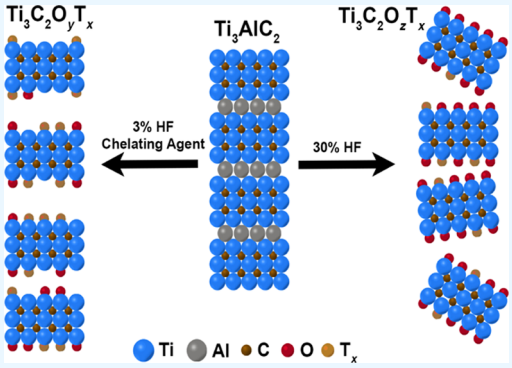

INTRODUCTION

Layered transition metal carbides, nitrides, and carbonitrides are a unique class of 2D materials that are promising for applications in battery electrodes,[1−4] CO_2 catalysis,[5,6] magnetic shielding,[7] and adsorption of heavy atoms.[8] These layered structures, known as MXenes, have a general formula $M_{n+1}X_nT_x$ (n = 1−4) and are comprised of an early transition metal M, e.g., Sc, Ti, Zr, Hf, V, Nb, Ta, Cr, or Mo, and a main group element X that is typically carbon and/or nitrogen. In MXenes, T_X denotes the surface terminating group on the basal planes, which is usually a mixture of −F, =O, and/or −OH.[9−11] MXenes are derived from a parent MAX phase, where the A layer (an element from groups 13 or 14) is selectively removed by exposing the compound to the appropriate etching conditions, and in the process, the layers are expanded. The most widely studied MXene, $Ti_3C_2T_x$, was first synthesized in 2011 by subjecting the MAX parent compound Ti_3AlC_2 to a concentrated solution (50%) of hydrofluoric acid (HF).[12] Following that discovery, the library of available MXenes has grown substantially as more combinations of ordered/disordered ($M_2'M''C_2T_x$ or $M_2'M_2''C_3T_x$) and solid solution MAX structures have been discovered experimentally or predicted theoretically.[13]

In order to maximize the utility of MXenes, it is important to navigate alternate chemistries that can selectively etch away the A layer while maintaining a low concentration of defects in the sheets and controlling the composition of the terminating functional groups, which is directly related to the etching method used.[14−16] The literature on this process describes a plethora of aqueous and nonaqueous etching methods. In etching processes that occur at or near ambient temperature, the use of different concentrations of HF (with 5% being the lowest concentration previously reported)[17] or *in situ* HF-producing chemicals have emerged as the principal methods for preparing MXenes.[18] Experimental methods have been developed that do not involve high concentrations of HF, but these entail the combination of fluoride salts with a strong acid (LiF/HCl, CoF_x/HCl, or FeF_3/HCl),[15,19−21] the use of bifluoride ammonium salts (NH_4HF_2),[22] Lewis acidic molten-salts ($ZnCl_2$, $CuCl_2$, $FeCl_2$, AgCl, $NiCl_2$, $CdCl_2$, or $CdBr_2$),[23−25] or hydrothermal etching in concentrated alkaline solutions.[26] These methods have had different degrees of success in completely removing the A atoms and controlling the termination of the layers. In general, they involve forcing conditions (high temperature, high pressure, and/or corrosive solvents) to carry out the reaction and in many cases result in incomplete conversion of the parent MAX phase.[27,28] MAX structures with larger n in $M_{n+1}AX_n$ require considerably longer etching times or stronger etchants to enable full conversion to MXenes.[29,30] Here, we re-examine the original HF etching

Received: September 26, 2023
Revised: October 5, 2023
Accepted: October 10, 2023
Published: October 24, 2023

https://doi.org/10.1021/acsomega.3c07442
ACS Omega 2023, 8, 41969−41976

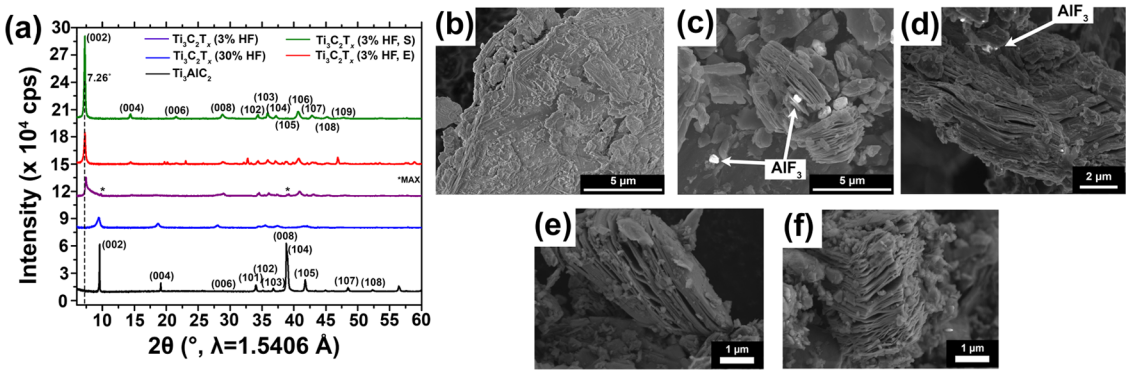

Figure 1. (a) X-ray diffraction patterns of Ti_3AlC_2 (black), MXene-30 (blue), MXene-3 (purple), MXene-E (red), and MXene-S (green). The use of HF at low concentration in tandem with a chelating agent results in a large increase in interlayer spacing while maintaining crystallinity. High-resolution scanning electron microscopy (HR-SEM) images of Ti_3AlC_2 (b), MXene-30 (c), MXene-3 (d), MXene-E (e), and MXene-S (f) showing the evolution from MAX crystals to lamellar MXenes. The characteristic accordion structure of all three MXene samples suggests a similar etching mechanism.

conditions by considering a room temperature and low concentration of HF in tandem with an aluminum chelating agent and evaluate the changes in the crystallinity and electronic structure of the products by using X-ray powder diffraction and X-ray absorption spectroscopy. The chelating agent used most successfully in this study is *N*,*N*′-dihydroxyoctanediamide (suberohydroxamic acid). As a multidentate hard Lewis base , this chelating agent has a high affinity for Al ions.[31] Because the resulting aluminum complexes are soluble and stable in aqueous weak acid solution, the method avoids the deposition of sparingly soluble AlF_3 that is the product of HF or fluoride salt/strong acid etching.

■ RESULTS AND DISCUSSION

Figure 1a shows X-ray powder diffraction (XRD) patterns of the MAX precursor Ti_3AlC_2, a sample etched at a high concentration (30% v/v, corresponding to a concentration of 17 M) of HF (labeled MXene-30), and samples etched at a low concentration (3% v/v, or 1.7 M, labeled MXene-3) HF and at low concentrations (3% v/v, or 1.7M) with the use of a chelating agent (labeled MXene-S for samples with suberohydroxamic acid and MXene-E for samples with EDTA). This more dilute etching solution still contains an excess of HF relative to the amount of aluminum present (about 17.5 F/Al). The X-ray powder diffraction (XRD) pattern of the MAX precursor can be assigned to the $p6\overline{3}mmc$ unit cell of Ti_3AlC_2.[12] After Ti_3AlC_2 is reacted with HF for 12 h, the intense diffraction peaks at 9.57,19.15, and 28.12°, corresponding to the (002), (004), and (006) reflections, shift to lower 2θ and become broader, indicating an increase in the interlayer spacing and a concomitant loss in crystallinity.[12] Additionally, the disappearance of the reflection at 38.93, which corresponds to the (104) reflection in the hexagonal structure of the MAX phase, is lost with the complete removal of the "A" layer to form $Ti_3C_2T_x$. The XRD pattern for MXene-3 (without a chelating agent) shows persistent peaks for the precursor at 9.67 and 38.93° in addition to broadened peaks similar to those of MXene-30. In comparison, the XRD patterns of samples made by reacting MAX with 3% v/v HF in the presence of a chelating agent after 36 h show sharp (002) reflections. Table 1 in the Supporting information shows the calculated values for the full width at half-maximum for the (002) reflection, depicting a significant difference between the MXene produced by reacting with HF and HF in the presence of chelating agent. For MXene-S and MXene-E, the (002) reflection is shifted from 9.57 in Ti_3AlC_2 to 7.25 2θ in stark contrast to the shift observed in MXene-30 from 9.57 to 9.39. The larger interlayer spacing of MXene-E and MXene-S (12.4 Å) is close to that found by the intercalation of ionic salts and organic compounds into MXenes and could be related to the intercalation of the chelating agents[4,16,32,33] or to hydration of the interlayer galleries since a peak with similar *d*-spacing is found for MXene-3. A least-squares refinement of the XRD patterns of MXene-E and MXene-S assigns the peaks at 7.26, 14.38, 21.48, and 28.82° to the (002), (004), (006), and (008) reflections, respectively.[34] Importantly, peaks corresponding to the (102), (103), (104), (106), (107), and (108) reflections can be easily distinguished at 34.37, 35.88, 37.19, 40.66, 42.83, and 45.18°, respectively, indicating retention of three-dimensional registry of the MXene sheets following the etching/intercalation process. The *a*, *b*, and *c* parameters for the refined hexagonal crystal structure of MXene-E and MXene-S were 3.03, 3.03, and 24.78 Å, respectively. The observations of sharp diffraction lines at high 2θ angles, h0l reflections, and expanded layer spacing indicate that low HF etching conditions preserve the atomic ordering of the MXene sheets. It is important to note that excessive amounts of the chelating agent inhibit the etching reaction; for this reason, the amounts of chelating agents used were carefully optimized.

In MXene-E, low-intensity unassigned reflections are related to agglomerates of the chelating agent on the MXene crystals, which can be seen in high-resolution scanning electron microscopy (HR-SEM, Figure 1e). Notably, these insoluble agglomerates are absent in the case of MXene-S. HR-SEM images of Ti_3AlC_2 (Figure 1b), MXene-30 (Figure 1c), MXene-3 (Figure 1d), MXene-E (Figure 1e), and MXene-S (Figure 1f) show the distinctive structural features of these materials. MXene-30 (Figure 1c) consists of accordion-like structures that are characteristic of MXenes made by etching Ti_3AlC_2 (Figure 1b). Figure 1c shows the presence of $AlF_3 \cdot 3H_2O$, which appears as bright nanoparticles in the image. The electronically insulating nature of these particles is suggested by their strong backscattering of electrons in the SEM image, and their high Al content is corroborated by energy dispersive spectroscopy (EDS) element mapping (Figure S1). Crystalline $AlF_3 \cdot 3H_2O$ nanoparticles have been observed as an undesired byproduct in HF or HF-producing synthetic methods (anhydrous AlF_3 solubility is 0.0053 g/L at 20

https://doi.org/10.1021/acsomega.3c07442
ACS Omega 2023, 8, 41969−41976

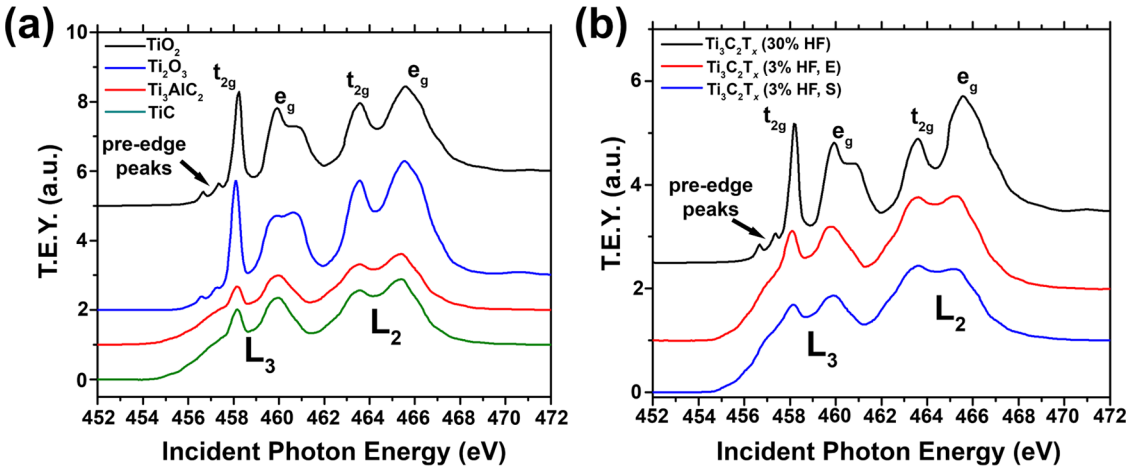

Figure 2. Ti L-edge X-ray absorption near-edge spectroscopy (XANES) for a series of benchmark Ti samples (a) that include TiO_2, Ti_2O_3, Ti_3AlC_2, and TiC, and for the MXenes synthesized by different etching methods (b). MXene-30 spectral features closely resemble those of TiO_2. In contrast, the MXene-E and MXene-S spectra resemble those of TiC and Ti_3AlC_2, suggesting that the rate of oxidation of the MXene layers using a low concentration of HF is slower than that at a high concentration.

°C).[12,19,21,35,36] The inconsistent formation of $AlF_3{\cdot}3H_2O$ particles has been shown to affect the distribution of interlayer spacings of $Ti_3C_2T_x$.[21] This can be directly observed in Figure 1c, where $AlF_3{\cdot}3H_2O$ significantly changes the interlayer distances in a localized area of the MXene while the rest of the structure is unaffected. Postsynthetic processes, such as repetitive filtration and centrifugation, can remove some of the AlF_3 deposited by chemical etching with concentrated HF. Nevertheless, the persistence of AlF_3 in SEM images indicates that it is not completely removed. The mechanism of formation for $AlF_3{\cdot}3H_2O$ was evaluated by Corbillon et al., who showed a direct correlation between the complexation equilibria of AlF^{2+}, AlF_2^{+}, AlF_3, AlF_4^{-}, AlF_5^{2-}, and AlF_6^{3-} and the ionic strength in the solution.[37] Cockreham et al. also studied the etching mechanism of MXenes with CoF_x/HCl and confirmed that the formation of $AlF_3{\cdot}3H_2O$ depends on the ionic strength of the solution and the concentration of fluoride ions, suggesting that there is a range of ionic strength conditions that promote the formation of $AlF_3{\cdot}3H_2O$.[21,37] In HR-SEM images of MXene-E and MXene-S (Figure 1e,f, respectively), the accordion-like structure is also retained, suggesting an etching mechanism similar to that in concentrated HF. However, $AlF_3{\cdot}3H_2O$ particles are not observed, consistent with the idea that Al is solubilized by the chelating agent. The smaller particles observed in Figure 1d,1e are the agglomerates of chelating agents on the MXene crystals that are also detected in the XRD pattern (Figure 1a).

The etching reaction that produces MXenes is slow, and with the chelating agents used here, at a low concentration of HF and ambient temperature, it requires 36 h to go to completion.[17,18] Figure S2 compares the XRD patterns of MXene-S and MXene-E under the same reaction conditions at a 12 h reaction time, where residual reflections of Ti_3AlC_2 show that the reaction is incomplete. As with other wet etching processes, etching of MAX phases is concentration-dependent,[1,38,39] where the rate increases with increasing concentration of etchant.[17] Density functional theory (DFT) calculations and *ab initio* molecular dynamics (AIMD) simulations performed by Srivastava et al. suggest that the intercalation of HF into the MAX structure and subsequent etching of the A layer requires a minimum of 7 HF molecules to extract one AlF_3.[40] In their proposed mechanism, protons and fluoride ions initially coordinate the Ti atoms at the edges of the crystal, weakening the Ti−Al bonds and facilitating the opening of the layers to further etch the Al layer. AIMD simulations indicated that at low concentrations of HF, fluoride ions bind to Al without forming AlF_3, suggesting that the etching process could be very slow under those conditions.[12,17,41] Our observations of a long etching time are consistent with their predictions. The chelating agent may serve to sequester Al species that are produced in the etching process but may not directly participate in the removal of Al from the edges of the MAX crystals.

Additionally, the passivating terminal groups may differ from those formed by the concentrated HF etching routes. It is important to note that the concentration and chemical nature of the etchant, which is correlated with the rate of etching, directly determine the stoichiometry and chemical nature of the terminal groups on MXene layers and the formation of defects.[42−45] For example, NMR studies of MXenes etched with concentrated HF vs LiF/HCl show differences in the stoichiometry of oxygen-terminated Ti in comparison to fluorine-terminated Ti.[44] X-ray photoemission spectroscopy (XPS) of $Ti_3C_2T_x$ samples etched in 50% hydrofluoric acid showed that the surface terminations consisted of a mixture of Ti−O, −F, and −OH (with adsorbed H_2O), with the predominant terminal group being −F for fresh MXene samples.[45] The authors additionally observed that as the sample ages in the air, the −F terminal groups are easily oxidized to oxyfluoride species, and the concentration of oxygen terminal groups increases considerably. For this reason, and to better understand the effects of the chelation etching method on the terminal groups of the MXene products, we employed X-ray absorption near-edge spectroscopy (XANES) to study the changes in the electronic structure of the material. As an element- and orbital-specific probe of unoccupied states, XANES is a valuable probe of the electronic structure and chemical bonding in extended solids.[46−48] We are especially interested in changes in the electronic structure of the Ti atoms since they relate directly to the chemical nature of the coordinated species. Moreover, for Ti_3AlC_2, the $Ti_3C_2T_x$ transformation has been shown to greatly affect the shape and energy of the Ti L-edge spectral signature. These changes are diagnostic of the changes in the terminating elements

https://doi.org/10.1021/acsomega.3c07442
ACS Omega 2023, 8, 41969−41976

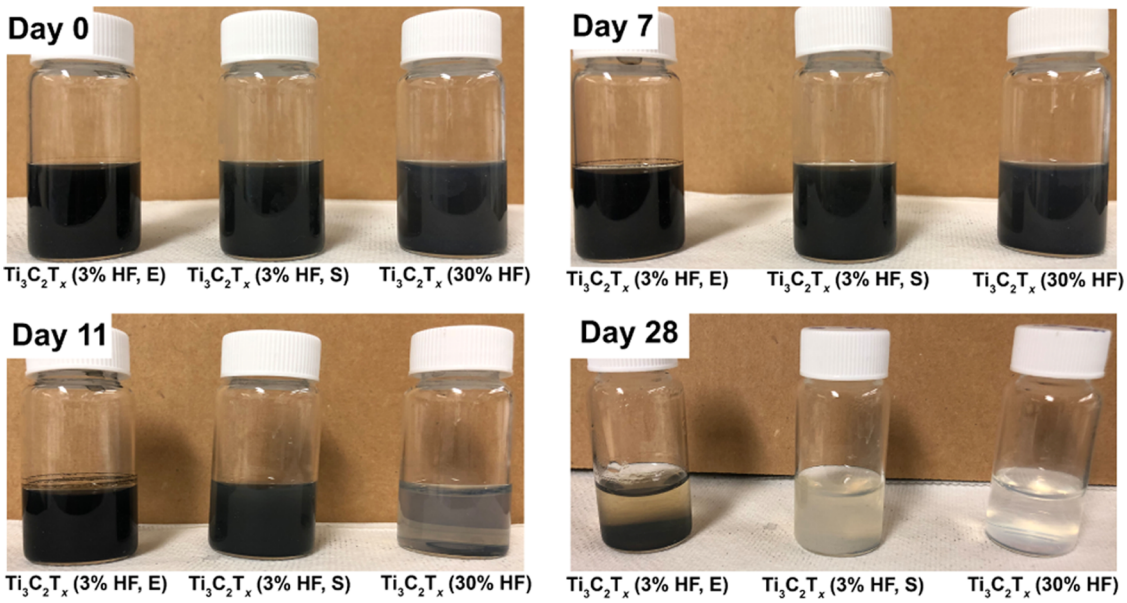

Figure 3. Photographs of MXene-30, MXene-E, and MXene-S samples in contact with air-saturated water for 0−28 days.

bound to Ti atoms on the basal planes of the MXene sheets, whereas the subsurface Ti atoms remain unchanged.[49] The Ti K-edge fingerprint (Figure S3) of the etched samples is characterized by a pre-edge peak at around 4.971 keV (transition of a 1s electron to the hybridized t_{2g} Ti 3d + C 2p and e_g Ti 3d + C 2p) and a main peak at around 4.985 keV (transition of a 1s electron to Ti 4p). While no major differences are apparent in the main peak, a loss in intensity can be observed in the pre-edge peak that is relatively independent of the etching method.[50]

The Ti L-edge XAS spectrum (Figure 2) is characterized by the Ti L_3 (approximately between 455 and 461 eV) and Ti L_2 (approximately between 462 and 465 eV) features that correspond to dipole allowed ($\Delta l = \pm 1$) transitions of Ti $2p^6 3d^0 \rightarrow 2p^5 3d^1$ electrons with spin $2p_{3/2}$ and $2p_{1/2}$, respectively. These features are split due to spin−orbital coupling of the Ti 2p atomic orbitals by approximately 4 eV.[51−54] The L_3 and L_2 transitions can be further split into doublet features due to symmetry considerations in the crystal field and the covalent or ionic interactions between the ligand and the transition metal center. For Ti (IV) oxides, these doublets are often described (for O_h or distorted O_h symmetry) as t_{2g} and e_g manifolds.[46,48,51] Moreover, L-edge spectra are dominated by coupling of the 3d electrons with the 2p core-hole, *i.e.*, the multiplet effect, and this phenomenon plays an important role in the broadening, spectral shape, and the L_3 to L_2 ratio of the spectral signature.[46,48,51,52,54,55] Figure 2a compares the Ti L-edge XANES spectra of TiO_2, Ti_2O_3, TiC, and Ti_3AlC_2. Here, we can discern clear differences in the electronic structure signature between titanium oxides and carbides. First, in TiO_2 and Ti_2O_3, the observed pre-edge features (456.6 and 457.3 eV) correspond to forbidden transitions within the dipole selection rule, which become allowed due to 2p-3d orbital mixing and, similarly to the Ti K-edge, are influenced by the geometry of the Ti polyhedron and the chemical nature of the ligand.[54,56] These pre-edge features cannot be easily distinguished in TiC and Ti_3AlC_2 samples because of broadening of the L_3 in carbide structures, which is attributed to the local crystal symmetry (rock-salt structure in TiC) and the orbital mixing between Ti and C atoms.[53] Unfortunately, an Auger decay process renders the Ti L_2 feature less informative due to an associated increase in spectral broadening.[52,53] Figure 2b compares the Ti L-edge XANES features of the MXene-30, MXene-S, and MXene-E samples. MXene-30 has an XAS signature that is virtually identical to that of TiO_2, confirming that the aqueous etching reaction using a high concentration of HF creates an oxidizing environment, and even with postsynthetic treatment of the product, oxidation of the basal planes affects the electronic structure of the material.[43] The Ti L-edge XANES signatures of MXene-S and MXene-E are quite similar to those of TiC and Ti_3AlC_2, indicating that the carbide-like bonding in the material is retained under milder etching conditions. Interestingly, the use of LiF/HCl significantly alters the electronic structure of $Ti_3C_2T_x$ relative to Ti_3AlC_2 in the Ti L-edge, but that spectrum does not show evidence of initial TiO_2 formation as the concentrated HF sample did in this study.[49] The XANES spectra thus are consistent with the XRD patterns, which suggested significant damage to the MXene sheets with etching in concentrated HF, forming a predominantly oxide terminating layer. In contrast, etching at a low concentration of HF in tandem with a chelating agent yields a MXene product in which the Ti atoms retain a predominantly carbide-like bonding environment. High-resolution X-ray photoelectron spectroscopy (XPS) of the Ti 2p, O 1s, C 1s, and Al 2p regions in Figure S4 provides some information about the relative amounts and chemical environments of elements at the outer (1−2 nm sampling depth) surface of the MXene samples.[45] Unfortunately, the spectra for MXene-E were affected by charging issues (likely related to the presence of the chelating agent), but the rough features of its spectra are similar to those of MXene-S. The Ti 2p and the C 1s regions show the presence of Ti oxycarbides and carbides in MXene-30 and MXene-S. In the XPS spectra (Figure S4d), both MXene-30 and MXene-S show a significant lowering of the Al 2p peak intensity compared to the MAX sample, indicating nearly complete removal of Al in these samples. In contrast, MXene-E shows a significant Al peak, likely resulting from the incomplete deposition of agglomerated chelating agents, as seen in Figure 1e. All of the etched samples show a binding

https://doi.org/10.1021/acsomega.3c07442
ACS Omega 2023, 8, 41969−41976

energy shift in the Al 2p peak, consistent with the removal of Al from the MAX phase and the formation of an Al^{3+} product. These observations are also supported by O K-edge (Figure S5) areas of high oxidation for MXene-30, whereas spectra of MXene-E and MXene-S resemble those of the TiC standard. Furthermore, Raman spectroscopy (Figure S6) measured at three different spots for the same sample demonstrates areas of high MXene characteristic and the presence of oxidation to TiO_2 in all three samples, but with MXene-30 being the most affected.

The relative stabilities of MXene samples prepared by different etching methods were also qualitatively compared. Approximately 0.100 g of each MXene powder was dispersed in a separate container of deionized water (d-H_2O), and the resulting air-saturated colloidal mixture was allowed to stand at room temperature under ambient conditions. Figure 3 shows photographs of these samples taken 0, 7, 11, and 28 days after dispersion of the MXene samples in water. No clear differences are observed between days 0 and 7, consistent with the observations of Zhang et al., who found that $Ti_3C_2T_x$ degraded after approximately 7 days.[43] On day 11, gray particles begin to appear in the solution above the MXene-30 solid; in contrast, dispersions of MXene-E and MXene-S retain the dark color of the MXene. During this transition period, the largest particles of MXene-30 settled to the bottom of the vial, and the colloids suspended in the solution above them appeared to be completely oxidized. This is similar to the trends observed by Zhang et al., where the rate of degradation depended on the size of the particles and where more than 85% of the sample was degraded after 10 days.[43] Interestingly, samples of MXene-E and MXene-S also consisted of larger particles and colloids suspended in solution, but the latter appeared stable. The oxidation of MXenes nucleates at the edges and propagates through the layers; this nucleation and growth is dependent on the amount of oxygen present in solution.[43] This is the reason why several approaches to inhibit the degradation of MXenes have relied on adding Ar to the colloidal solution or on suspending the solid in an organic solvent.[43,57] After 28 days, all three samples showed gray or a mixture of gray and black colloids that are characteristic of oxidation to TiO_2. Figure S7 shows the XRD patterns for MXene-30, MXene-E, and MXene-S samples dispersed in deionized H_2O at 28 days. For all of the samples, the XRD patterns are characterized by reflections that can be assigned to anatase or rutile TiO_2; interestingly, none of the XRD patterns retained any reflections of $Ti_3C_2T_x$. For MXene-30 and MXene-S, the XRD patterns show the formation of both anatase and rutile TiO_2. In contrast, the XRD pattern for MXene-E shows no crystalline phase, suggesting that the product is amorphous TiO_2. The metastability of $Ti_3C_2T_x$ is a well-known shortcoming of this material and remains a subject of research.[20,42,43,58] While it is clear that the milder etching method does not prevent the eventual oxidation and hydrolysis of MXenes to TiO_2, it does show increased resistance to degradation relative to materials made by etching in concentrated HF.

■ CONCLUSIONS

In summary, we have presented an alternative route to an archetypical MXene with the use of low concentrations of HF in conjunction with aluminum chelating agents. MXenes have in a short time become uniquely functional materials for electronic, energy, and catalytic applications. The chelation method may serve as a useful synthetic tool for producing carbide-like MXenes from other M, A, and X elements in order to explore their properties and applications.

■ MATERIALS AND METHODS

Synthesis of MXenes. The MXene-30 samples were prepared as described in the literature.[12,17] Approximately 0.0025 mol of Ti_3AlC_2 MAX powder (purchased from Carbon-Ukraine, Y-Carbon, Ltd.) was carefully mixed with an aqueous solution of hydrofluoric acid (*caution:* concentrated HF is extremely hazardous). All experiments were carried out in polystyrene test tubes. HF (45% v/v in water) was purchased from Fisher Scientific, diluted to 30% v/v concentration in a total volume of 30 mL, and reacted with the MAX sample at room temperature for 12 h. The resulting powder was washed with copious amounts of deionized water by vacuum filtration, which was followed by resuspension water and centrifugation at 9000 rpm for 25 min until the measured pH was close to neutral. The powder was then dried in a vacuum oven overnight. The MXene-E and MXene-S samples were prepared by carefully mixing approximately 0.0025 mol of Ti_3AlC_2 MAX solid with an aqueous solution of 3% v/v HF (36 h) and 3% v/v HF with ethylenediaminetetraacetic acid (EDTA) tetrasodium salt, dihydrate (Acros Organics, 99%, CAS: 10378-23-1), or suberohydroxamic acid (Sigma-Aldrich, 95%, CAS: 38937-66-5), respectively, at room temperature for 12 or 36 h in a total volume of 30 mL. The chelating agent was added prior to the addition of HF. The molar amounts of chelating agent were 0.0012 mol of ethylenediaminetetraacetic acid tetrasodium salt, dihydrate in MXene-E, and 0.00020 mol of suberohydroxamic acid in MXene-S. These amounts were optimized by varying the amounts of chelating agents. The resulting powders were similarly washed with copious amounts of deionized water by vacuum filtration followed by resuspension and centrifugation in water at 9000 rpm for 25 min until the measured pH was close to neutral. A 0.01 M NaOH solution was used to remove the unreacted chelating agent. The powder was then dried in a vacuum oven overnight.

Characterization Methods. X-ray diffraction patterns were acquired by using a Rigaku SmartLab SE with an automated multipurpose X-ray diffractometer, a D/tex Ultra 250 detector, and a copper X-ray source (1.5406 Å), using a step size of 0.01, acquisition speed of 3.0/min, and an incident slit of 1/2 mm. Full width at half-maximum (fwhm) values were calculated using a single peak fit gauss function as implemented in OriginPro 2023 software. A Zeiss Supra 50VP SEM was used to obtain high-magnification images of the treated powders at an accelerating voltage of 5 kV and in the secondary electron mode of detection; EDS maps were acquired at an operating voltage of 15 kV. A ND-MDT confocal Raman spectrometer, with a 532 nm excitation wavelength laser, 3 mW power, objective 100×, exposure time of 30 s, and a Peltier-cooled Andor CCD detector, was used for Raman measurements. Before Raman measurements, the samples were pressed into a pellet for acquisition. Ti L-edge and O K-edge X-ray absorption spectroscopy were conducted at beamline 29-ID IEX of the Advanced Photon Source, Argonne National Laboratory. Data were collected at a pressure lower than 1×10^{-8} Torr in total electron yield (TEY) using a microchannel plate from 450 to 480 eV (Ti L-edge) and 520 to 580 eV (O K-edge). We used circular polarization with an overall energy resolution better than 500 meV. Calibration of the samples was carried out by using TiO_2 as a reference. The TEY was pre- and postedge normalized by

https://doi.org/10.1021/acsomega.3c07442
ACS Omega 2023, 8, 41969−41976

using the incident X-ray intensity (I_0) using the drain current from a gold mesh upstream of the sample as implemented by the Athena suite. Ti K-edge X-ray absorption spectroscopy was taken at the 5-BM-D in transmission mode, Si(111) detector, 0.2 eV step size. The measurements were calibrated and pre- and postedge normalized by using Ti metal as a reference and as applied by the Athena suite. XPS experiments were performed using a Physical Electronics VersaProbe II instrument equipped with a monochromatic Al kα X-ray source ($h\nu$ = 1486.7 eV) and a concentric hemispherical analyzer. Charge neutralization was performed using both low-energy electrons (<5 eV) and argon ions. The binding energy axis was calibrated using sputter-cleaned Cu (Cu $2p_{3/2}$ = 932.62 eV, Cu $3p_{3/2}$ = 75.1 eV) and Au foils (Au $4f_{7/2}$ = 83.96 eV). Peaks were charge referenced to the CH_x band in the carbon 1s spectra at 284.8 eV. Measurements were made at a takeoff angle of 45° with respect to the sample surface plane. This resulted in a typical sampling depth of 3−6 nm (95% of the signal originated from this depth or shallower). Quantification was done using instrumental relative sensitivity factors (RSFs) that account for the X-ray cross section and inelastic mean free path of the electrons.

■ ASSOCIATED CONTENT

Supporting Information

The Supporting Information is available free of charge on the ACS Publications Web site. The Supporting Information is available free of charge at https://pubs.acs.org/doi/10.1021/acsomega.3c07442.

> X-ray powder diffraction line widths; EDS element maps; X-ray diffraction comparison of samples etched 12 h; Ti K-edge X-ray absorption spectra; O K-edge X-ray absorption spectra; Raman spectra of etched samples; X-ray diffraction patterns of samples exposed to water (PDF)

■ AUTHOR INFORMATION

Corresponding Authors

Luis R. De Jesús Báez − *Department of Chemistry, University of Pennsylvania, Philadelphia, Pennsylvania 19104, United States; Department of Chemistry, University at Buffalo, Buffalo, New York 14260, United States*; Email: ldjesus@buffalo.edu

Thomas E. Mallouk − *Department of Chemistry, University of Pennsylvania, Philadelphia, Pennsylvania 19104, United States*; orcid.org/0000-0003-4599-4208; Email: mallouk@sas.upenn.edu

Authors

Alyssa S. Rosas − *Department of Chemistry, Pennsylvania State University, University Park, Pennsylvania 16802, United States*

Pratibha Mahale − *Department of Chemistry, University of Pennsylvania, Philadelphia, Pennsylvania 19104, United States*; orcid.org/0000-0002-3163-4386

Complete contact information is available at: https://pubs.acs.org/10.1021/acsomega.3c07442

Author Contributions

The study was designed by L.R.D.J.B. and T.E.M. L.R.D.J.B., A.S.R., and P.M. carried out the experiments, and the manuscript was written through contributions of all authors. All authors have given approval to the final version of the manuscript.

Funding

This work was supported by the National Science Foundation under grant DMR-1952877. L.R.D.J.B. acknowledges support from the Eberly College of Science Postdoctoral Fellowship program at Pennsylvania State University and from the Provost Postdoctoral Fellowship program at the University of Pennsylvania. A.S.R. acknowledges the Alfred P. Sloan Foundation and the National GEM Consortium for fellowship funding. Part of this work was performed at the DuPont-Northwestern-Dow Collaborative Access Team (DND-CAT) located at Sector 5 of the Advanced Photon Source (APS). DND-CAT is supported by Northwestern University, The Dow Chemical Company, and DuPont de Nemours, Inc. This research used resources of the Advanced Photon Source, a U.S. Department of Energy (DOE) Office of Science User Facility operated for the DOE Office of Science by Argonne National Laboratory under Contract No. DE-AC02-06CH11357.

Notes

The authors declare no competing financial interest.

■ ACKNOWLEDGMENTS

The authors gratefully acknowledge the help provided by Dr. Jessica McChesney and Dr. Fanny Rodolakis during the soft X-ray absorption measurements at the 29-ID-D beamline and the help from the Advance Photon Source at the Argonne National Laboratory. The authors appreciate Jeff Shallenberger for XPS measurements and help in analysis. The authors also thank the Centralized Research Facility of Drexel University for the use of the SEM. This work was supported by the National Science Foundation under grant DMR-1952877.

■ REFERENCES

(1) Anasori, B.; Lukatskaya, M. R.; Gogotsi, Y. 2D Metal Carbides and Nitrides (MXenes) for Energy Storage. *Nat. Rev. Mater.* **2017**, *2* (2), 16098.

(2) Liang, X.; Garsuch, A.; Nazar, L. F. Sulfur Cathodes Based on Conductive MXene Nanosheets for High-Performance Lithium-Sulfur Batteries. *Angew. Chem., Int. Ed.* **2015**, *54* (13), 3907−3911.

(3) Wang, Y.; Li, Y.; Qiu, Z.; Wu, X.; Zhou, P.; Zhou, T.; Zhao, J.; Miao, Z.; Zhou, J.; Zhuo, S. Fe3O4@Ti3C2MXene Hybrids with Ultrahigh Volumetric Capacity as an Anode Material for Lithium-Ion Batteries. *J. Mater. Chem. A* **2018**, *6* (24), 11189−11197.

(4) Xu, M.; Lei, S.; Qi, J.; Dou, Q.; Liu, L.; Lu, Y.; Huang, Q.; Shi, S.; Yan, X. Opening Magnesium Storage Capability of Two-Dimensional MXene by Intercalation of Cationic Surfactant. *ACS Nano* **2018**, *12* (4), 3733−3740.

(5) Zhang, X.; Zhang, Z.; Li, J.; Zhao, X.; Wu, D.; Zhou, Z. Ti2CO2MXene: A Highly Active and Selective Photocatalyst for CO2 Reduction. *J. Mater. Chem. A* **2017**, *5* (25), 12899−12903.

(6) Low, J.; Zhang, L.; Tong, T.; Shen, B.; Yu, J. TiO_2/MXene Ti_3C_2 Composite with Excellent Photocatalytic CO_2 Reduction Activity. *J. Catal.* **2018**, *361*, 255−266.

(7) Iqbal, A.; Shahzad, F.; Hantanasirisakul, K.; Kim, M. K.; Kwon, J.; Hong, J.; Kim, H.; Kim, D.; Gogotsi, Y.; Koo, C. M. Anomalous Absorption of Electromagnetic Waves by 2D Transition Metal Carbonitride Ti3CNTx(MXene). *Science* **2020**, *369* (6502), 446−450.

(8) Peng, Q.; Guo, J.; Zhang, Q.; Xiang, J.; Liu, B.; Zhou, A.; Liu, R.; Tian, Y. Unique Lead Adsorption Behavior of Activated Hydroxyl Group in Two-Dimensional Titanium Carbide. *J. Am. Chem. Soc.* **2014**, *136* (11), 4113−4116.

(9) Gogotsi, Y.; Anasori, B. The Rise of MXenes. *ACS Nano* **2019**, *13* (8), 8491−8494.

(10) Deysher, G.; Shuck, C. E.; Hantanasirisakul, K.; Frey, N. C.; Foucher, A. C.; Maleski, K.; Sarycheva, A.; Shenoy, V. B.; Stach, E. A.; Anasori, B.; Gogotsi, Y. Synthesis of Mo_4VAlC_4MAX Phase and Two-Dimensional Mo4VC4MXene with Five Atomic Layers of Transition Metals. *ACS Nano* **2020**, *14* (1), 204−217.
(11) Naguib, M.; Mochalin, V. N.; Barsoum, M. W.; Gogotsi, Y. 25th Anniversary Article: MXenes: A New Family of Two-Dimensional Materials. *Adv. Mater.* **2014**, *26* (7), 992−1005.
(12) Naguib, M.; Kurtoglu, M.; Presser, V.; Lu, J.; Niu, J.; Heon, M.; Hultman, L.; Gogotsi, Y.; Barsoum, M. W. Two-Dimensional Nanocrystals Produced by Exfoliation of Ti_3AlC_2. *Adv. Mater.* **2011**, *23* (37), 4248−4253.
(13) Sokol, M.; Natu, V.; Kota, S.; Barsoum, M. W. On the Chemical Diversity of the MAX Phases. *Trends Chem.* **2019**, *1* (2), 210−223.
(14) Karlsson, L. H.; Birch, J.; Halim, J.; Barsoum, M. W.; Persson, P. O. Å. Atomically Resolved Structural and Chemical Investigation of Single MXene Sheets. *Nano Lett.* **2015**, *15* (8), 4955−4960.
(15) Sang, X.; Xie, Y.; Lin, M. W.; Alhabeb, M.; Van Aken, K. L.; Gogotsi, Y.; Kent, P. R. C.; Xiao, K.; Unocic, R. R. Atomic Defects in Monolayer Titanium Carbide (Ti3C2Tx) MXene. *ACS Nano* **2016**, *10* (10), 9193−9200.
(16) Hart, J. L.; Hantanasirisakul, K.; Lang, A. C.; Anasori, B.; Pinto, D.; Pivak, Y.; van Omme, J. T.; May, S. J.; Gogotsi, Y.; Taheri, M. L. Control of MXenes' Electronic Properties through Termination and Intercalation. *Nat. Commun.* **2019**, *10* (1), No. 522, DOI: 10.1038/s41467-018-08169-8.
(17) Alhabeb, M.; Maleski, K.; Anasori, B.; Lelyukh, P.; Clark, L.; Sin, S.; Gogotsi, Y. Guidelines for Synthesis and Processing of Two-Dimensional Titanium Carbide ($Ti_3C_2T_x$ MXene). *Chem. Mater.* **2017**, *29* (18), 7633−7644.
(18) Lim, K. R. G.; Shekhirev, M.; Wyatt, B. C.; Anasori, B.; Gogotsi, Y.; Seh, Z. W. Fundamentals of MXene Synthesis. *Nat. Synth.* **2022**, *1* (8), 601−614.
(19) Wang, X.; Garnero, C.; Rochard, G.; Magne, D.; Morisset, S.; Hurand, S.; Chartier, P.; Rousseau, J.; Cabioc'H, T.; Coutanceau, C.; Mauchamp, V.; Célérier, S. A New Etching Environment (FeF3/HCl) for the Synthesis of Two-Dimensional Titanium Carbide MXenes: A Route towards Selective Reactivity: Vs. Water. *J. Mater. Chem. A* **2017**, *5* (41), 22012−22023.
(20) Lipatov, A.; Alhabeb, M.; Lukatskaya, M. R.; Boson, A.; Gogotsi, Y.; Sinitskii, A. Effect of Synthesis on Quality, Electronic Properties and Environmental Stability of Individual Monolayer Ti3C2MXene Flakes. *Adv. Electron. Mater.* **2016**, *2* (12), 1600255.
(21) Cockreham, C. B.; Zhang, X.; Li, H.; Hammond-Pereira, E.; Sun, J.; Saunders, S. R.; Wang, Y.; Xu, H.; Wu, D. Inhibition of AlF3·3H2O Impurity Formation in Ti3C2Tx MXene Synthesis under a Unique CoFx/HCl Etching Environment. *ACS Appl. Energy Mater.* **2019**, *2* (11), 8145−8152.
(22) Halim, J.; Lukatskaya, M. R.; Cook, K. M.; Lu, J.; Smith, C. R.; Näslund, LÅ.; May, S. J.; Hultman, L.; Gogotsi, Y.; Eklund, P.; Barsoum, M. W. Transparent Conductive Two-Dimensional Titanium Carbide Epitaxial Thin Films. *Chem. Mater.* **2014**, *26* (7), 2374−2381.
(23) Li, M.; Lu, J.; Luo, K.; Li, Y.; Chang, K.; Chen, K.; Zhou, J.; Rosen, J.; Hultman, L.; Eklund, P.; Persson, P. O. Å.; Du, S.; Chai, Z.; Huang, Z.; Huang, Q. Element Replacement Approach by Reaction with Lewis Acidic Molten Salts to Synthesize Nanolaminated MAX Phases and MXenes. *J. Am. Chem. Soc.* **2019**, *141* (11), 4730−4737.
(24) Li, Y.; Shao, H.; Lin, Z.; Lu, J.; Liu, L.; Duployer, B.; Persson, P. O. Å. Å.; Eklund, P.; Hultman, L.; Li, M.; Chen, K.; Zha, X.-H. H.; Du, S.; Rozier, P.; Chai, Z.; Raymundo-Piñero, E.; Taberna, P.-L. L.; Simon, P.; Huang, Q. A General Lewis Acidic Etching Route for Preparing MXenes with Enhanced Electrochemical Performance in Non-Aqueous Electrolyte. *Nat. Mater.* **2020**, *19* (8), 894−899.
(25) Kamysbayev, V.; Filatov, A. S.; Hu, H.; Rui, X.; Lagunas, F.; Wang, D.; Klie, R. F.; Talapin, D. V. Covalent Surface Modifications and Superconductivity of Two-Dimensional Metal Carbide MXenes. *Science* **2020**, *369* (6506), 979−983.
(26) Li, T.; Yao, L.; Liu, Q.; Gu, J.; Luo, R.; Li, J.; Yan, X.; Wang, W.; Liu, P.; Chen, B.; Zhang, W.; Abbas, W.; Naz, R.; Zhang, D. Fluorine-Free Synthesis of High-Purity Ti3C2Tx (T = OH, O) via Alkali Treatment. *Angew. Chem., Int. Ed.* **2018**, *57* (21), 6115−6119.
(27) Kim, Y. J.; Kim, S. J.; Seo, D.; Chae, Y.; Anayee, M.; Lee, Y.; Gogotsi, Y.; Ahn, C. W.; Jung, H. T. Etching Mechanism of Monoatomic Aluminum Layers during MXene Synthesis. *Chem. Mater.* **2021**, *33* (16), 6346−6355.
(28) Cockreham, C. B.; Goncharov, V. G.; Hammond-Pereira, E.; Reece, M. E.; Strzelecki, A. C.; Xu, W.; Saunders, S. R.; Xu, H.; Guo, X.; Wu, D. Energetic Stability and Interfacial Complexity of Ti3C2TxMXenes Synthesized with HF/HCl and CoF2/HCl as Etching Agents. *ACS Appl. Mater. Interfaces* **2022**, *14* (36), 41542−41554, DOI: 10.1021/acsami.2c09669.
(29) Anasori, B.; Shi, C.; Moon, E. J.; Xie, Y.; Voigt, C. A.; Kent, P. R. C.; May, S. J.; Billinge, S. J. L.; Barsoum, M. W.; Gogotsi, Y. Control of Electronic Properties of 2D Carbides (MXenes) by Manipulating Their Transition Metal Layers. *Nanoscale Horiz.* **2016**, *1* (3), 227−234.
(30) Anasori, B.; Xie, Y.; Beidaghi, M.; Lu, J.; Hosler, B. C.; Hultman, L.; Kent, P. R. C.; Gogotsi, Y.; Barsoum, M. W. Two-Dimensional, Ordered, Double Transition Metals Carbides (MXenes). *ACS Nano* **2015**, *9* (10), 9507−9516.
(31) Evers, A.; Hancock, R. D.; Martell, A. E.; Motekaitis, R. J. Metal Ion Recognition in Ligands with Negatively Charged Oxygen Donor Groups: Complexation of Fe(III), Ga(III), In(III), Al(III), and Other Highly Charged Metal Ions. *Inorg. Chem.* **1989**, *28* (11), 2189−2195.
(32) Luo, J.; Zhang, W.; Yuan, H.; Jin, C.; Zhang, L.; Huang, H.; Liang, C.; Xia, Y.; Zhang, J.; Gan, Y.; Tao, X. Pillared Structure Design of MXene with Ultralarge Interlayer Spacing for High-Performance Lithium-Ion Capacitors. *ACS Nano* **2017**, *11* (3), 2459−2469.
(33) Simon, P. Two-Dimensional MXene with Controlled Interlayer Spacing for Electrochemical Energy Storage. *ACS Nano* **2017**, *11* (3), 2393−2396.
(34) Appleman, D. E. Job 9214: Indexing and Least-Squares Refinement of Powder Diffraction Data *US Geological Survey, Computer Contribution 20, US National Technical Information Service, Document PB-16188* 1973.
(35) Rajavel, K.; Ke, T.; Yang, K.; Lin, D. Condition Optimization for Exfoliation of Two Dimensional Titanium Carbide (Ti3C2Tx). *Nanotechnology* **2018**, *29* (9), No. 095605, DOI: 10.1088/1361-6528/aaa687.
(36) States, U. Aluminum Fluoride *Cold Spring Harb. Protoc.* 2006; Vol. *2006* 5. pdb.caut2442.
(37) Corbillon, M. S.; Olazabal, M. A.; Madariaga, J. M. Potentiometric Study of Aluminium-Fluoride Complexation Equilibria and Definition of the Thermodynamic Model. *J. Solution Chem.* **2008**, *37* (4), 567−579.
(38) Judge, J. S. A Study of the Dissolution of SiO[Sub 2] in Acidic Fluoride Solutions. *J. Electrochem. Soc.* **1971**, *118* (11), 1772.
(39) Deckert, C. A. Etching of CVD Si3 N 4 in Acidic Fluoride Media. *J. Electrochem. Soc.* **1978**, *125* (2), 320−323.
(40) Srivastava, P.; Mishra, A.; Mizuseki, H.; Lee, K. R.; Singh, A. K. Mechanistic Insight into the Chemical Exfoliation and Functionalization of Ti3C2MXene. *ACS Appl. Mater. Interfaces* **2016**, *8* (36), 24256−24264.
(41) Mashtalir, O.; Naguib, M.; Dyatkin, B.; Gogotsi, Y.; Barsoum, M. W. Kinetics of Aluminum Extraction from Ti3AlC2 in Hydrofluoric Acid. *Mater. Chem. Phys.* **2013**, *139* (1), 147−152.
(42) Persson, I.; Halim, J.; Hansen, T. W.; Wagner, J. B.; Darakchieva, V.; Palisaitis, J.; Rosen, J.; Persson, P. O. Å. How Much Oxygen Can a MXene Surface Take Before It Breaks? *Adv. Funct. Mater.* **2020**, *30*, No. 1909005, DOI: 10.1002/adfm.201909005.
(43) Zhang, C. J.; Pinilla, S.; McEvoy, N.; Cullen, C. P.; Anasori, B.; Long, E.; Park, S. H.; Seral-Ascaso, A.; Shmeliov, A.; Krishnan, D.; Morant, C.; Liu, X.; Duesberg, G. S.; Gogotsi, Y.; Nicolosi, V.

Oxidation Stability of Colloidal Two-Dimensional Titanium Carbides (MXenes). *Chem. Mater.* **2017**, *29* (11), 4848−4856.
(44) Hope, M. A.; Forse, A. C.; Griffith, K. J.; Lukatskaya, M. R.; Ghidiu, M.; Gogotsi, Y.; Grey, C. P. NMR Reveals the Surface Functionalisation of Ti3C2MXene. *Phys. Chem. Chem. Phys.* **2016**, *18* (7), 5099−5102.
(45) Halim, J.; Cook, K. M.; Naguib, M.; Eklund, P.; Gogotsi, Y.; Rosen, J.; Barsoum, M. W. X-Ray Photoelectron Spectroscopy of Select Multi-Layered Transition Metal Carbides (MXenes). *Appl. Surf. Sci.* **2016**, *362*, 406−417.
(46) Stohr, J. *NEXAFS Spectroscopy*; Springer, 1992.
(47) Henderson, G. S.; de Groot, F. M. F.; Moulton, B. J. A. X-Ray Absorption Near-Edge Structure (XANES) Spectroscopy. *Rev. Mineral. Geochem.* **2014**, *78* (1), 75−138.
(48) Chen, J. G. NEXAFS Investigations of Transition Metal Oxides, Nitrides, Carbides, Sulfides and Other Interstitial Compounds. *Surf. Sci. Rep.* **1997**, *30* (1−3), 1−152, DOI: 10.1016/S0167-5729(97)00011-3.
(49) Yang, Y.; Hantanasirisakul, K.; Frey, N. C.; Anasori, B.; Green, R. J.; Rogge, P. C.; Waluyo, I.; Hunt, A.; Shafer, P.; Arenholz, E.; Shenoy, V. B.; Gogotsi, Y.; May, S. J. Distinguishing Electronic Contributions of Surface and Sub-Surface Transition Metal Atoms in Ti-Based MXenes. *2D Mater.* **2020**, *7* (2), 025015 DOI: 10.1088/2053-1583/ab68e7.
(50) Lukatskaya, M. R.; Bak, S. M.; Yu, X.; Yang, X. Q.; Barsoum, M. W.; Gogotsi, Y.Probing the Mechanism of High Capacitance in 2D Titanium Carbide Using in Situ X-Ray Absorption Spectroscopy *Adv. Energy Mater.* 2015; Vol. *5* DOI: 10.1002/aenm.201500589.
(51) De Groot, F. M. F.; Fuggle, J. C.; Thole, B. T.; Sawatzky, G. A. L2,3 x-Ray-Absorption Edges of D0 Compounds: K+, Ca2+, Sc3+, and Ti4+ in Oh (Octahedral) Symmetry. *Phys. Rev. B* **1990**, *41* (2), 928−937.
(52) Kroll, T.; Solomon, E. I.; de Groot, F. M. F. Final-State Projection Method in Charge-Transfer Multiplet Calculations: An Analysis of Ti L-Edge Absorption Spectra. *J. Phys. Chem. B* **2015**, *119* (43), 13852−13858.
(53) de Groot, F. M. F.; Figueiredo, M. O.; Basto, M. J.; Abbate, M.; Petersen, H.; Fuggle, J. C. 2 p X-Ray Absorption of Titanium in Minerals. *Phys. Chem. Miner.* **1992**, *19* (3), 140−147.
(54) De Groot, F. M.; Fuggle, J. C.; Thole, B. T.; Sawatzky, G. A. 2p X-Ray Absorption of 3d Transition-Metal Compounds: An Atomic Multiplet Description Including the Crystal Field. *Phys. Rev. B* **1990**, *42* (9), 5459−5468.
(55) Groot, F. De. Multiplet Effects in X-Ray Spectroscopy. *Coord. Chem. Rev.* **2005**, *249* (1−2), 31−63.
(56) Jiang, N.; Su, D.; Spence, J. C. Determination of Ti Coordination from Pre-Edge Peaks in Ti K -Edge XANES. *Phys. Rev. B* **2007**, *76* (21), No. 214117, DOI: 10.1103/PhysRevB.76.214117.
(57) Maleski, K.; Mochalin, V. N.; Gogotsi, Y. Dispersions of Two-Dimensional Titanium Carbide MXene in Organic Solvents. *Chem. Mater.* **2017**, *29* (4), 1632−1640.
(58) Bhat, A.; Anwer, S.; Bhat, K. S.; Mohideen, M. I.; Liao, K.; Qurashi, A. Prospects Challenges and Stability of 2D MXenes for Clean Energy Conversion and Storage Applications. *npj 2D Mater. Appl.* **2021**, *5* (1), 61.

https://doi.org/10.1021/acsomega.3c07442
ACS Omega 2023, 8, 41969−41976